



46

47

48 **1 Introduction**

49

50 The concentration, size, shape, and the degree of rounding of glacial ice-transported blocks of rock
51 may change with distance from the source outcrop. Spatial trends in concentration have been used
52 frequently to indicate preferred ice flow directions (Kujansuu & Saarnisto, 1990; Evans, 2007, Benn &
53 Evans, 2011, p. 675). Concentrated bands of ice-freighted erratics are referred to as 'indicator plumes',
54 'indicator trains' or 'indicator fans', with concentrations dropping off rapidly outside of the plumes
55 due to ice-flow induced dispersion (Larson & Mooers, 2004). None-the-less, concentration is also
56 sustained by comminution, whereby blocks fracture, or abrade to form smaller blocks and fragments
57 through time and distance from the source outcrop. In contrast to dispersion, there has been less
58 focus on changes in size, shape, and edge-rounding with distance from source (Benn & Evans, 2011).
59 The changes in the shape of blocks are functions of the mechanical properties of the blocks, primarily
60 rock strength and structure, as well as the physical processes promoting comminution. A change in
61 block shape also represents a change in block size. To explore the controls on edge rounding and the
62 shape of erratics, dispersal from a well-known exposure of the Shap granite (Sg) in the UK was
63 examined in the present study. Improved understanding of process controls related to edge rounding
64 and fracture should shed light on the associated basal ice dynamics related to block form changes
65 generally. The two key issues are: 1) the relative importance of fracture mechanics in reducing block
66 size in contrast to edge-rounding and 2: whether edge-rounding and shape coevolve with distance
67 from the source outcrop.

68

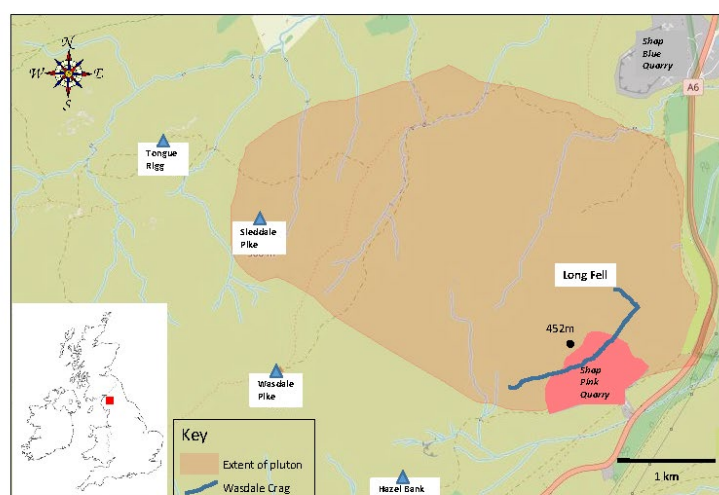
69 **1.1 The Study Area and Context of the Study**

70

71 The exposure of the Sg pluton occupies a small area (c., 7 km²) in the eastern English Lake District (Fig.
72 1) defining a distinct, small, source area for granite blocks. The variation in the concentrations of Sg
73 blocks with distance from the pluton has been used as a key indicator of the directions of ice



74 movement across northern England (reviewed by Carling *et al.*, 2013) during the Dimlington Stadial
75 (*c.*, 30 ka BP to 14.7 ka BP) within the overall period of the Devensian glaciation (*c.*, 33 ka BP to 11.3
76 ka BP). Around the Late Glacial maximum (LGM: 26.5 ka BP to 19 ka BP, Clark *et al.*, 2009), the region
77 was covered by ice, several hundred metres thick (Evans *et al.*, 2009), and Sg blocks were entrained
78 from the subglacial bedrock. Long Fell, on the eastern margin of the exposed pluton, is a kilometre-
79 scale *r*oches moutonnées, severely ice-plucked in the east and south-east at Wasdale Crag (Fig. 1), with
80 smooth, ice-planned surfaces occurring to the north, west and on the summit (point 452m), indicating
81 the erosional effects of moving ice and debris (Hallet, 1981). The west to east change in the style of
82 erosion, from smoothing to plucking, is consistent with ice in the vicinity of the pluton moving
83 predominately to the east in an early phase (*c.*, 29-25 ka BP; Livingstone *et al.*, 2012; Merritt *et al.*,
84 2019) of the Dimlington Stadial, and generally northwards across the pluton subsequent to 22 ka BP,
85 *i.e.* towards the end of the LGM (Livingstone *et al.*, 2012; Merritt *et al.*, 2019); the latter supposition
86 consistent with the W.S.W. to E.N.E. orientation of glacial striations on the pluton (Nicolson, 1868).
87



88

89 *Figure 1: Location of the Shap granite pluton. The central portion of the ice-plucked outcrop (Wasdale*
90 *Crag) crag has been destroyed by quarrying. Base map is from © OS Map Local data.*

91



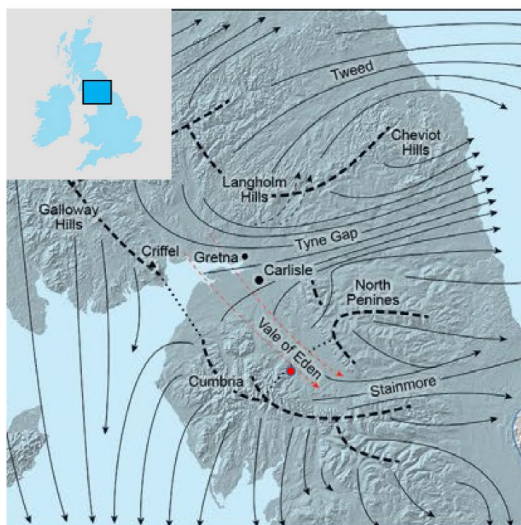
92 In terms of concentration, the dominant dispersal of Sg erratics, during the early phase of the
93 Dimlington Stadial (Stage I; 29-25 ka BP; Merritt *et al.*, 2019) was eastward (Carling *et al.*, 2013) within
94 sustained ice flow through the topographically controlled corridor of the Stainmore gap across the
95 north Pennines hills (Fig. 2A). The plume extended as far as the east coast of England; a distance more
96 than 100km (Fig. 3). Block size tends to diminish with distance, although examples of far-travelled
97 large blocks occur sparingly (Carling *et al.*, 2023). Due to shifting ice divides and competing ice
98 dispersal centres (Merritt *et al.*, 2019), subsequently two Sg plumes dispersed in southerly directions
99 until, in the late stadial, erratics briefly were dispersed northwards from the vicinity of the pluton
100 (Carling *et al.*, 2013) in accord with the ice movements reported by Livingstone *et al.* (2012). These
101 latter dispersal directions are not considered further herein. The focus solely is on those erratics the
102 final transport vectors of which are due east, defining a simple linear direction over which changes in
103 the nature of the erratic populations might be measured.

104

105 Less well understood than directions of travel and changes in concentration, is the process of edge-
106 rounding and shape changes of Sg blocks that accompany size reduction. The granite is an ideal choice
107 for study as the composition and texture is uniform (Grantham, 1929), mostly giving a massive,
108 unlayered, structure to individual blocks. Layering, such as found within sedimentary rocks, would
109 add complexity to the study of shape evolution, which complexity is avoided in this study. Hopkins
110 (1849) had commented briefly on the rounding of Sg blocks (density ~ 2.61 tonnes m^{-3}) as size reduces
111 towards the east coast, yet such rapid changes in form are seemingly at odds with the high strength
112 of the rock. The strength of Sg in compression exceeds 207 MPa (Holland, 1959;

113

114



115

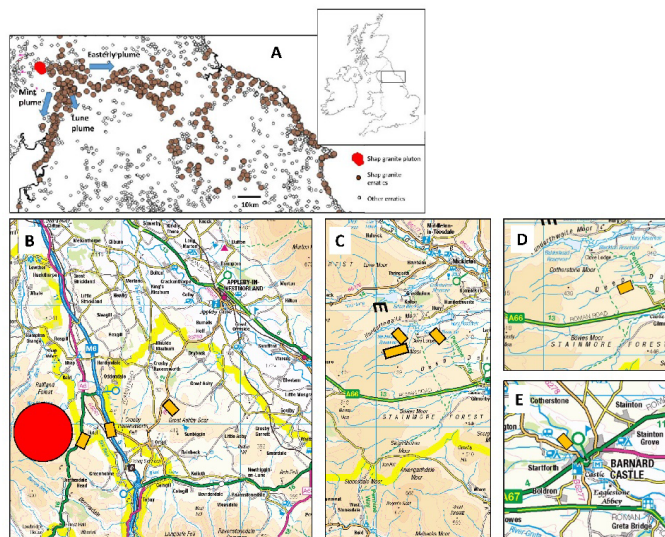
116

117 *Figure 2: Reconstructed of Stage I (29-25 ka BP) of the last British-Irish Ice Sheet around the Solway*
118 *Firth (from Merritt et al., 2019. Reproduced with permission) in northern England Stage (inset panel).*
119 *Eastward ice flow through prominent topographic corridors occurs across the north Pennines. Broken*
120 *and dotted lines refer to ice divides. Arrows indicate ice-flow vectors (dotted arrows indicate*
121 *alternative ice-flow scenarios). Topography from NEXTMap digital elevation data. Shap granite erratic*
122 *plume dispersed to the east from the pluton (red dot) chiefly over Stainmore (see Fig 3).*
123

124 Day & Goudie, 1977; Goudie, 2006) such that the rock is considered ‘very strong’ (British Standards,
125 1981). Despite the rock strength, Hodgson (1870) had remarked on how seemingly rapid rounding of
126 granite might be aided by rock friability due to a high mica content associated primarily with biotite
127 (Firman, 1953). Biotite is soft compared with the large phenocrysts of feldspars and quartz (Firman,
128 1953) that dominate the granite composition. Nevertheless, there has been no investigation of the
129 changes in shape and rounding of Sg blocks with distance from the source; with very few granite blocks
130 visually maintaining significant mass over 10’s of km. A study of blocks exposed on the modern land
131 surface, away from major watercourses, should reveal rock-wear processes associated with glacial
132 transport as there has been negligible losses to Sg surfaces due to post-glacial subaerial weathering
133 (Parsons & Lee, 2005). Consequently, an hypothesis was proposed: ‘Sg ice-transported blocks would



134 *display systematic changes in edge-rounding and shape’; with an aim ‘to demonstrate if edge rounding*
135 *and shape coevolve with distance to the east from the pluton’.*



136

137 *Figure 3: A) Spatial distribution of examples of Shap granite erratics within the study area,*
138 *showing the early easterly-directed plume, the southerly Mint and Lune plumes and subsequent*
139 *movement of some erratics northwards just east of the pluton. Location of sampling sites (yellow*
140 *rectangles); B) Wasdale Bridge, Haybanks, Blasterfield C) upper Teesdale; D) Levy Pool; E)*
141 *Barnard Castle. Base maps based on © OS 1:250 000 Scale Colour Raster™.*

142 Shape (and size) changes in a Shap granite block occur due to three predominant processes which
143 scale from effecting small areas of a block to larger areas:

144

145 1) abrasion, whereby grain-size fragments (e.g., phenocrysts) are ground-off the block surface
146 (Haldorsen, 1981; Benn & Evans, 2011) primarily by shear stresses associated with blocks
147 moving across a bedrock or till surface in the direction of basal ice motion, or by ice and till
148 moving over stationary blocks lodged against the substratum - this process can result in
149 distinct rounded surfaces on a block (Boulton, 1978; Hallet, 1979);

150

151 2) spallation, whereby flakes of rock are freed from the surface of the block (Olsen, 1983) due
152 to externally-derived and internally-derived tensile deviatoric stresses in the rock, both



153 imposed by the motion of the ice overburden, with the shear stresses acting on planes at less
154 than the block scale (Li *et al.*, 2018) – this process reduces block mass but results in localized
155 scarred surfaces;

156

157 3) fracture (Buscarnera & Einav, 2021) whereby the ‘parent’ block splits into substantial parts
158 (often two; here referred to as ‘child’ products). The propagating fissure ultimately may be
159 due to compression loading but, at the block surface, it is the result of a tensile stress (acting
160 on a plane at block scale) flexing the stoss surface of a brittle block lying on a hard basal surface,
161 leading to fissure development often transverse to the direction of basal ice motion (Morland
162 & Boulton, 1975; Hallet, 1996; Benn & Evans, 2011, p264). The tensile strength of a rock is
163 typically an order of magnitude less than the compressive strength (Li *et al.*, 2018). This
164 tripartite classification informed the Method.

165

166 To address the hypothesis, the focus of the study is abrasion and fracture, but observations on
167 spallation were obtained for completeness, with the latter results reported within Supplementary
168 Information. There is justification from studies of bedrock outcrop erosion by basal ice that both the
169 degree of abrasion of bedrock surfaces and the number of fracture events are related to time in
170 transport (Cohen *et al.*, 2006) and thus the distance erratics are moved.

171

172 **2 Method**

173

174 Shap granite blocks were sampled along a west to east transect, starting from below Wasdale Crag. It
175 was assumed that all the sampled blocks were from the same population subject to basal traction
176 transport (*vis.* Boulton, 1978) for much of the transport histories; the population being a coarser
177 component of a lodgement till deposited during the waning phase of the easterly phase of ice motion
178 (Hallet, 1979). Blocks ($L > c.$, 1.0 m) were located by field walking. Locations sampled include Wasdale
179 Old Bridge, Haybanks, Blasterfield, sites near Barnard Castle in Teesdale and Levy Pool near Brough



180 (Table S1), respectively 0.8 km, 3.5 km, 8.4 km, *c.*, 36 km and *c.*, 41 km from the Wasdale Crag outcrop
181 (Fig. 3). To obtain similar sample sizes, the areas searched for the final two locations necessarily
182 increased as the surface density of blocks decreased eastwards. Examples of erratics were selected
183 that were sitting on exposed bedrock or till surfaces, so as not to be partially buried. Distance from
184 the source outcrop is assumed to relate to time in transport.

185 At each location, edge, and shape measurements and scar enumeration were made on thirty blocks
186 as briefly described below; the full procedure developed within Supplementary Information. The
187 sample size was found to be sufficient for the aims of the project. These data were supplemented by
188 a regional shape data compendium (Carling *et al.*, 2013). Changes in block size with distance from the
189 pluton are not considered herein using field data, as a statistically significant sample size at each
190 location would have to be prohibitively large to reflect the complete size range of blocks. Rather block
191 size changes are considered within a theoretical framework related to shape changes. Blocks are
192 considered as cuboids consisting of *faces* and *edges*.

193 In accord with 1) abrasion: edge rounding was measured after Wentworth (1923). In brief, each of
194 the three most tightly rounded edges on the visible portion of each block was defined by a chord (l),
195 delimiting a segment of the block beneath each rounded edge, to give between 80 and 90 values for
196 each location. Consideration of the height (h) of the segment in relation to the chord length
197 constrains the radius (r_c) of an inscribed circle beneath the rounded edge, which radius is a measure
198 of the degree of rounding:

199

$$200 \quad r_c = \frac{l^2}{8h} + \frac{h}{2} \quad (1)$$

201

202 The radius of curvature reduces as the chord length reduces towards zero and often a right-angle
203 corner occurs when r_c approaches 0. More rounded blocks have larger radii of curvature than less
204 rounded blocks as the sizes of the inscribed circles increase as edges become less sharp. In similar



205 fashion, the edge rounding was measured for joints bounding *in situ* Shap granite blocks constituting
206 the outcrop of Wasdale Crag. These latter data provide a base line of the degree of edge rounding of
207 blocks which have been subject to ice abrasion in place, but without subsequent transport.

208

209 To consider 3) shape changes by fracture: from initial field reconnaissance, blocks close to the source
210 often appear cubic, but polyhedrons occur sparingly - ranging from wedges to prisms. Further
211 from the source more ellipsoidal forms are evident. Consequently, to obtain an indication of the shape
212 of a cuboid or an ellipsoid block, the lengths of the three orthogonal axes: long axis (L); medium axis
213 (M) and the short axis (S) were recorded in the field – polyhedrons were not sampled – to give c., 30
214 values for each location. Consideration of the mechanics of shape changes also sheds light on the size
215 reduction process with distance. Fracture within individual blocks is sometimes associated with joints
216 and other block-scale planes of weakness. Yet, ice compressive force is the predominant mechanism
217 for significant progressive change in shape for homogeneous granite blocks, inducing tensile fracture
218 and block size reduction. Shape and size changes were examined either via a stochastic fracture model,
219 applicable to fracture at right-angles to either of the L , M or S axes (Domokos *et al.*, 2015) of ellipsoidal
220 blocks or, in accord with the silver ratio model applicable to cuboid blocks fracturing across the M -axis
221 alone (Buscarnera & Einav, 2021), as is explained in the Results.

222

223 **3 Results**

224 **3.1 Edge rounding**

225 As is evident from the form of equation 1, rounding is a positive function of the square of the length
226 of the chord of the segment, l , and an inverse function of the segment height, h (Fig. 4). As the
227 inscribed radius values are obtained from both the values of l and h (Equation 1), there is an element
228 of co-variance between the two axes in both panels A and B of Fig. 4. However, plotting the data in
229 this manner allows ready visualization of the trends of the radius data (r_c) relative to the variation in

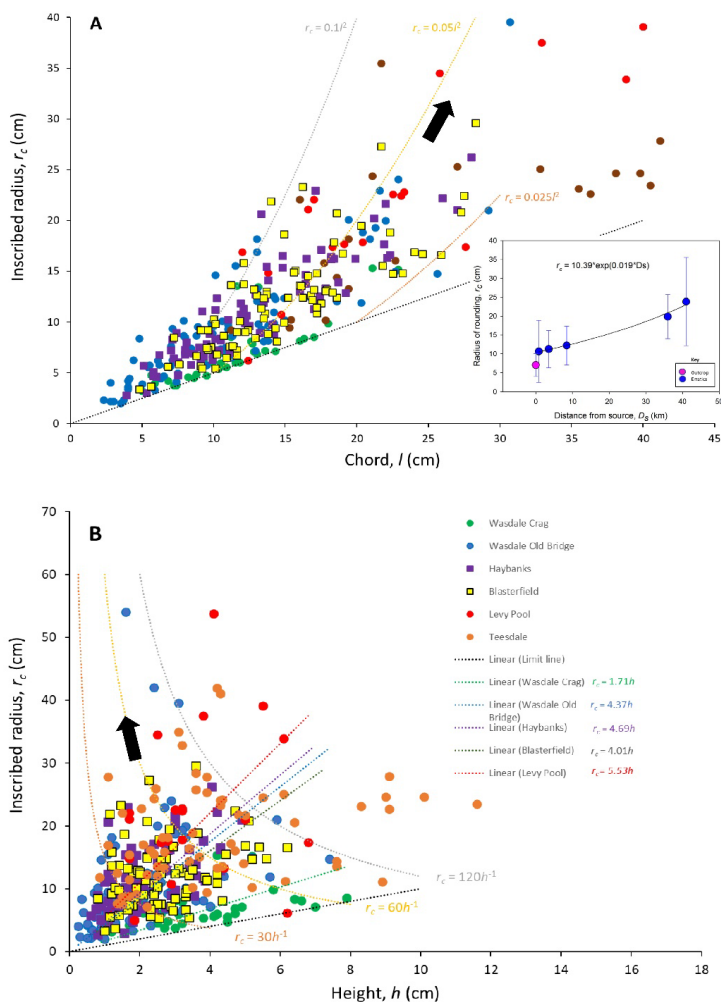


230 the controlling parameters (l, h). Lower limits to data plotting positions occur in both panels equal to:

231 $r_c = l/2$ and $r_c = h$ respectively.

232 The joint rounding on the pluton is less developed in comparison with the rounding of edges of blocks
233 only 0.8km away at Wasdale Old Bridge (Fig. 4). Although the range in heights of the segments are
234 similar for both locations, the range in chord lengths for the pluton includes smaller values giving
235 overall 'sharper' average edge profiles for the pluton joints in contrast to the Wasdale Old Bridge
236 blocks. It is evident that any 'parent' blocks newly entrained from the outcrop will exhibit both lightly
237 rounded joint edges (glacially abraded when *in situ*) as well as sharp, fresh edges, the latter due to
238 fracture upon release from the outcrop. However, although the initial lightly rounded edges can be
239 further rounded with distance, fracture of entrained blocks introduces new 'sharp' edges as detailed
240 next.

241 Although as distance increases larger radii are more frequent, small radii also occur at distance (Fig.
242 4). It is unlikely that small radii can survive abrasive transport over several 10's of km from the pluton,
243 rather repeated fracture introduces new sharp edges and thus new small radii to different generations
244 of blocks. These new sharp edges begin to round far from the pluton. Although the plots of Fig. 4 are
245 developed considering singular data points from many blocks, if the trends are considered to
246 represent the rounding evolution that would occur for individual blocks, then the black arrows indicate
247 the general direction of edge rounding evolution (*i.e.*, Fig. 4 panel A: if h is constant and l is variable;
248 panel B: if l is constant and h is variable). The linear functions in Fig. 4B allow ready comparison
249 between locations such that, for any value of h , the degree of edge rounding is more pronounced with
250 distance from the pluton; specifically, the linear curves (green, blue, purple, and red) have increasing
251 values of the constant (*i.e.*, 1.71, 4.37, 4.69; 5.53 respectively). Similar linear functions for values of l
252 can be applied to Fig. 4A but, for the sake of clarity, these curves are not plotted. The detail of edge



253

254 *Figure 4: Trends in the values of the inscribed radius as a function of: A) chord length, and; B) segment*
 255 *height. Black arrows indicate the direction of travel of the hypothetical function for an individual block*
 256 *(see main text). Examples of hypothetical curves (brown, yellow and grey) for the trends in individual*
 257 *clast evolution are given for both $r_c \propto l^2$ and $r_c \propto h^{-1}$. Key in panel B also applies to panel A. Inset*
 258 *panel shows mean and s.d. of edge rounding as function of distance from outcrop.*

259

260 rounding is considered within the Discussion, as edge-rounding of individual blocks is not a smooth

261 function of distance from the source as might be inferred from the black arrows in Fig. 4 and from the

262 inset figure of mean edge rounding with distance from the outcrop (Fig. 4 inset panel). The latter



263 figure depicts an exponential increase in the mean radius of curvature with distance (D_s) from the
264 source outcrop:

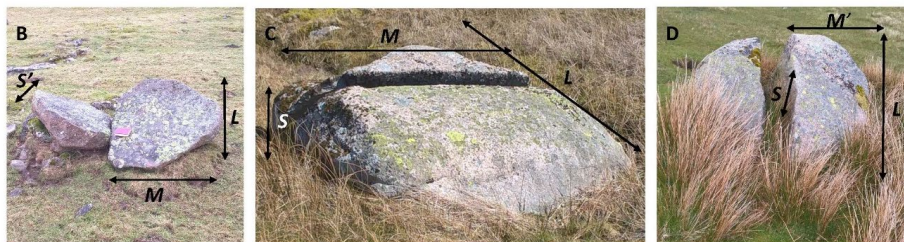
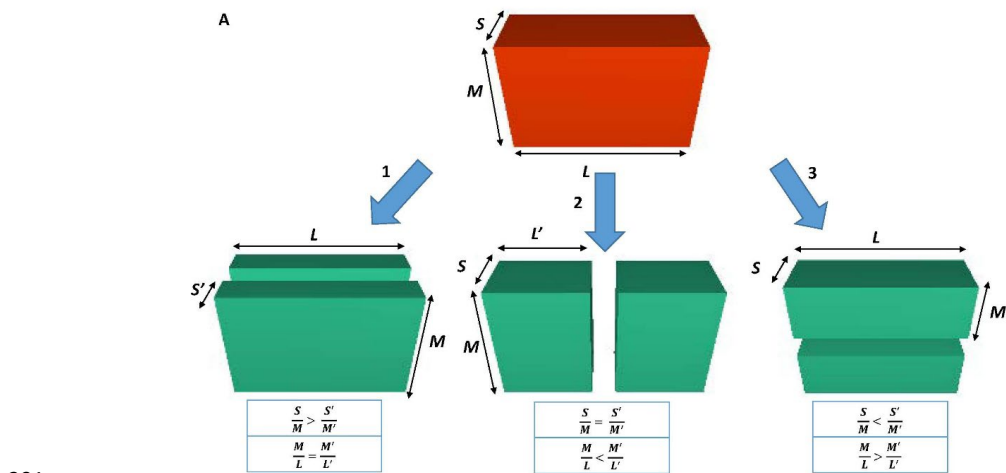
$$265 \quad r_c = 10.3881e^{(0.0194D_s)} \quad (2)$$

266 3.2 Shape evolution

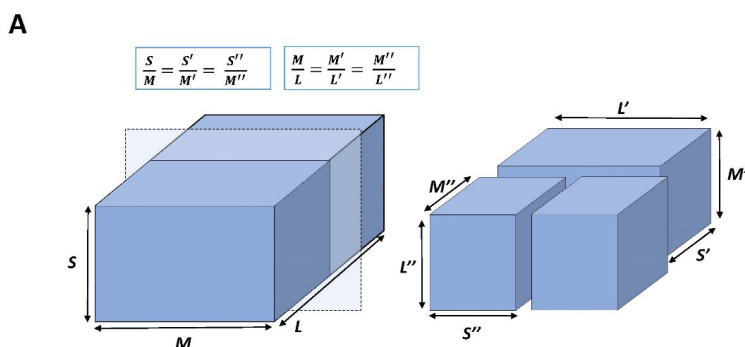
267 In the context of natural hexahedrons, the *stochastic model* of progressive fracture due to the stress
268 of compression (Domokos *et al.*, 2015), describes the generation of ellipsoids with the orthogonal axes
269 length proportions: 2.32; 1.52: 1 (Fig. 5A), whereas the *silver ratio* progressive fracture model
270 (Buscarnera & Einav, 2021) describes the generation of cuboids with the edge length proportions: $\sqrt[3]{2^2}$;
271 $\sqrt[3]{2}$; 1, *i.e.*; 1.59: 1.26: 1 (Fig. 6A). In the former model, a fracture plane is orthogonal to any of the
272 three sides of a cuboid (enclosing the ellipsoid) and separates two pieces of equal mass. In the silver
273 ratio model, a fracture plane occurs orthogonal to the current longest axis, separating two pieces of
274 equal mass. In nature, deviation from these two models can occur such that shape self-similarity, in
275 terms of axial ratios, is not maintained necessarily upon successive fracture events if the subsequent
276 fracture is across an axis that differs from the previous fracture event. Fracture across the plane of
277 the short axis was observed in nature (Fig. 5B). However, systematic fracture across the plane of the
278 long axis (Fig. 5C) and across the medium axis (Fig. 5D; Fig. 6B) appeared predominant (*vis* Benn, 1992)
279 for the blocks observed in the field, in accord with both the stochastic and silver models. Given that
280 most blocks rest with the short axis vertical, fracture across the L or M axes is consistent with known
281 fracture mechanics, whereby the centre of an object is the location, under loading, of the maximum
282 in the tensile stress and the consequent nucleation point for fracture (Hiramatsu & Oka, 1966; Shipway
283 & Hutchings, 1993). From this point, a fracture line develops to the block edges (Man *et al.*, 2018)
284 transverse to the direction of tensile loading. For low values of static or dynamic loading, the rock
285 eventually ruptures into two parts (Man *et al.*, 2018). Thus, although a block on occasion might
286 fracture across an axis at variance with the two models above, there is a tendency for blocks to evolve



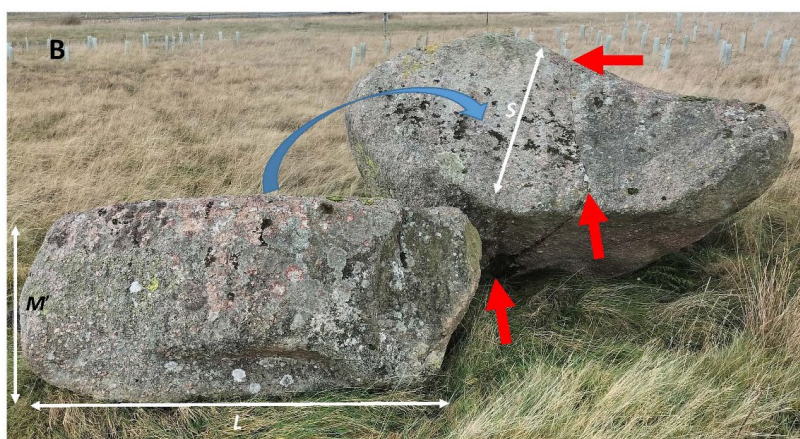
287 towards one or the other model. The system state attractors for these two models are shown in Fig.
 288 7, wherein natural block shapes are considered. Importantly, compression and tensile fracture leads
 289 in both models initially to uniquely defined anisotropic forms, although isotropic forms ($L = M = S$) can
 290 occur in principle with progressive fracture if the fracture rule in each model is relaxed and varied.



293 *Figure 5: A) Schematic representation of the concept of the stochastic fracture model applied to a*
 294 *three-dimensional cuboid (enclosing an ellipsoid – see Fig. S1) subject to successive fracture given an*
 295 *assumed identical stress loading to the granite block at each fracture event. Fracture planes are*
 296 *orthogonal to a side and separate two pieces of equal mass. Shape self-similarity is not maintained*
 297 *upon successive fracture events. Three different fracture styles are possible within the model, as*
 298 *labelled 1, 2 and 3; B) Example of a well-rounded block split along a fracture plane consistent with*
 299 *model 1; C) Example of a well-rounded block split along a fracture plane consistent with model 2; D)*
 300 *Example of a well-rounded block split along a fracture plane consistent with model 3. The long axes*
 301 *are foreshortened in panels B, C and D.*

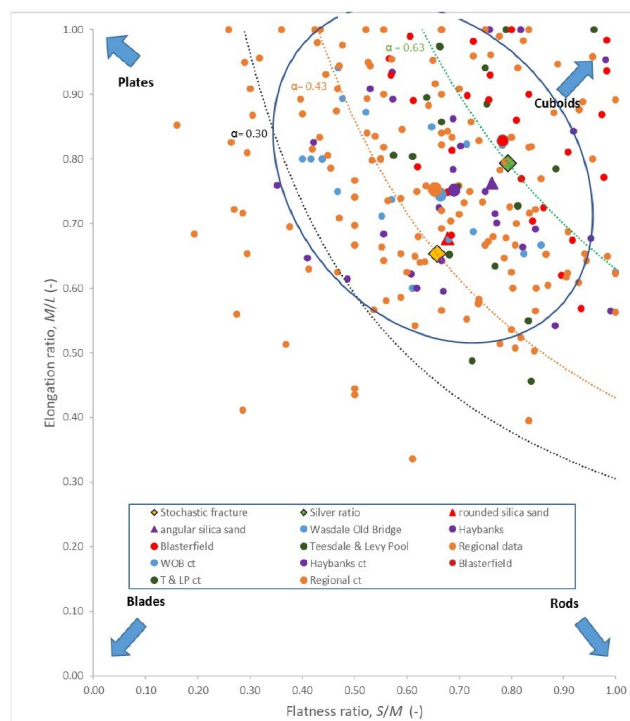


302



303

304 *Figure 6: A) Schematic representation of the concept of the silver ratio model applied to a three-*
 305 *dimensional cuboid (– see Fig. S1) subject to successive fracture given an assumed identical direction*
 306 *of stress loading to the granite block at each fracture event. Fracture planes are orthogonal to the*
 307 *current long axis. Shape self-similarity is more closely maintained (in contrast to Fig. 5) upon successive*
 308 *fracture events; B) Example of silver ratio block. Block to left is approximately the same size as the*
 309 *block to the right and the lower surface (not seen) was originally on the top surface of the right-hand*
 310 *block with the exposed failure plane bisecting the M-axis alignment of the original parent block. The*
 311 *red arrows delineate a fracture plane, aligned with the M-axis of the right-hand block, which divides*
 312 *the right-hand block into two near-equal halves.*
 313



314

315 *Figure 7: The shape relationship for blocks in terms of the Zingg (1935) ratios. The system state*
 316 *attractors for stochastic fracture (gold diamond) and silver ratio (green diamond) are shown, as are*
 317 *the central tendency shapes for mechanically crushed silica sand grains that were initial sub-rounded*
 318 *or angular (Seo et al., 2021). Curves represent the trend in values of M/L and S/M for constant*
 319 *values of S/L. ct symbols represent the central tendency of each population. Oval is the 95% contour*
 320 *after Oakey et al., 2005.*

321

322 Within Fig. 7 the Zingg ratios (S/M and M/L) for the sampled locations are plotted together with a data
 323 set for the broader region (Regional data). Within Fig. 7 completely equant (isotropic) forms are
 324 absent and plate-like forms survive more readily than rods. Nonetheless, the central tendency of block
 325 shape within the regional data is $S/M = 0.65$ and $M/L = 0.75$; *i.e.*, roughly midway between the system
 326 state attractor for stochastic fracture and the silver ratio attractor. Lines of constant equal aspect
 327 ratios (S/L) are shown for the silver ratio model ($\alpha = 0.63$) and for the stochastic fracture model ($\alpha =$
 328 0.43). Seo *et al.* (2021) showed that for homogeneous silica grains, fracture depended on initial
 329 particle form (Fig. 7) with angular grains tending towards the silver ratio whilst rounded grains tended



330 towards stochastic fracture. If the fracture process is scale-invariant, then the size differences
331 between silica grains and the Shap blocks can be ignored, and one would expect the Shap granite (a
332 largely homogeneous lithology) to migrate across the diagram from silver to stochastic fracture as
333 cubic blocks become progressively more rounded and ellipsoidal. Blocks deviating from either model
334 (either too long or flat, *e.g.*, approaching $\alpha = 0.30$), will tend to fracture and migrate back towards $\alpha =$
335 0.43, as is especially evident in Fig. S6B. The central tendencies of the regional data and each of the
336 sampled locations are closely grouped between the central tendencies of the silver and stochastic
337 fracture. The exception is the Blasterfield location which lies closer to the silver ratio, but with
338 increased distance of transport, Teesdale & Levy Pool blocks are in accord with stochastic fracture.
339 Thus, it is evident that block fracture fluctuates between each model, with a trend for constant equal
340 aspect ratios close to $\alpha = 0.50$ (not plotted in Fig. 7).

341 Although Fig. 7 provides an impression of the spread of block shapes around a central tendency there
342 is no clear impression of the actual shape evolution as possible representative shapes can only be
343 selected arbitrarily from the data clouds. Further, only the cube (or sphere) limit point (*e.g.*, 1, 1 in
344 Fig. 7) is real. Limit points for rods and plates exist only through mathematical definition, because as
345 the rod and plate limit points are approached, rods become infinitely long and plates infinitely thin.
346 Thus, representative shapes need to be selected objectively. To solve this problem the procedure of
347 Oakey *et al.* (2005) was utilized to define representative shapes that define the 95% contour around
348 the central tendency of the regional data, represented by the blue oval in Fig. 7. With reference to the
349 position of the 95% contour in the blade quadrant, curve $\alpha = 0.30$ is selected to demarcate a lower
350 bound for common block ratios; with a few plate-like or rod-like blocks occurring in the lower portion
351 of the diagram.

352

353 **3.3 Size evolution**



354 The size distribution of the Shap granite blocks with distance from the pluton source has not received
355 detailed attention, although Carling *et al.* (2013) provide some general observations suggesting there
356 is size reduction with distance. In this study, the sample sizes were insufficient to demonstrate the
357 reduction in block size expected with distance from the source outcrop. However, controls on size
358 reduction are evident. Specifically, blocks greater than $L = 4\text{m}$ are rare (Carling *et al.*, 2013), the size
359 being controlled by the close joint spacing of the granite at source (Firman, 1953). With few
360 exceptions, large blocks ($L > 3.0\text{ m}$) do not occur beyond 7 km from the pluton, at which point medium
361 blocks ($2.5 > L > 1.5\text{ m}$) become scarce, with small blocks ($1.5 > L > 0.5\text{ m}$) and cobble-sized material
362 dominating with further dispersal (Carling *et al.*, 2013). These observations indicate that there was a
363 control on the upper size of blocks entrained from the pluton and fracture rapidly reduced block size
364 inducing a crude size-reduction down plume within just a few kilometres. This process was
365 accompanied by local deposition of abrasion and spallation debris as components of lodgement till.
366 Nevertheless, the fracture mechanics that control block shape inevitably control size evolution (Figs.
367 5 and 6). For example, fracturing a parent cube with 4m long edges and its progeny across the L -axis,
368 only six sequent fracture divisions are required to produce a 1 m cube, as will be demonstrated in the
369 Discussion.

370

371 **4 Discussion: The context of size and shape constraints**

372

373 The initial hypothesis proposed that Sg ice-transported blocks would display changes in edge-rounding
374 and shape with distance to the east from the pluton. As shown in the Results and elaborated below
375 edge-rounding does change with distance but block shape is conservative.

376

377 Space-time substitution is an underlying tenant of this study, in that the size and shape characteristics
378 of multiple individual blocks (an erratic plume), dispersing across the landscape, can reflect the



379 evolution of a single erratic block through time along the same general spatial trajectory. An adequate
380 number of sampled blocks are required for this analogy to hold because perturbations to the
381 population of erratics can occur during dispersal. For example, blocks can have been introduced to
382 the W-E trajectory of the study plume by N-S ice movements reworking blocks previously deposited
383 outside of the eastern-directed plume during periods of time after the main W-E ice flow. Also, for
384 the purposes of determining transport distance, a zero x-axis origin has been assumed to be the most
385 easterly outcrop of the pluton at Wasdale Crag. However, some blocks might have been sourced up
386 to a few kilometres to the west of Wasdale Crag. Despite these potential perturbations, the small
387 sample sizes are sufficient to clearly demonstrate systematic change in edge rounding as well as block
388 shape evolution. Finally, edge-rounding and shape are re-set to a degree for the children each time a
389 parent block fractures, so the process of rounding and shape adjustment is not a smooth function of
390 distance from the outcrop, as is explained below.

391

392 **4.1 A conceptual model of block edge rounding controls**

393

394 It should be acknowledged that this study has not considered abrasion of the faces of blocks but has
395 focussed on the edges which tend to abrade and round more rapidly than the associated faces
396 (Boulton, 1974). The edges of blocks still within the outcrop are sharp, albeit some are subject to a
397 slight degree of rounding in place (Fig. 4). Detached blocks close to the outcrop also tend to exhibit
398 slightly ice-rounded edges, with sharply angled joint planes characterising the other faces due to
399 fracture release of the block from outcrop. The increase in edge rounding with distance confirms the
400 initial hypothesis.

401

402 Block edge rounding initially is constrained by the hardness of the Shap granite and the way it fractures
403 when first entrained at outcrop. The absence of significant edge rounding at the outcrop indicates
404 that blocks were entrained continually until the imposed stresses fell below that required to quarry



405 further blocks. Otherwise, edge rounding of entrained blocks is associated with basal traction
406 transport (Boulton, 1978; Hallet, 1979). Although the compressive strength of granite is high, the
407 tensile strength is an order of magnitude lower; possible as low as 4% of the compressive strength,
408 *i.e.*, 8 MPa (Anikoh *et al.*, 2015; Demirdag *et al.*, 2018; Engineering ToolBox, 2008). Thus, where
409 compression is translated into flexure, the propensity of the block to elongate across the axis of flexure
410 leads readily to fracture of the brittle granite. This condition means that many blocks close to source
411 initially exhibited near right-angle edges (Fig. 4). Given this geometric constraint, radii of edge
412 curvature inevitable are small initially, approaching the limit: $r_c = l/2$ and $r_c = h$, and increase with
413 distance from the outcrop due to abrasion. However, fracture away from the outcrop introduces new
414 sharp edges (Figs. 4 & 7), such that larger radii characterizing an individual edge-rounded block just
415 before fracture are augmented by smaller radii. This change is reflected in the scatter of radii values
416 found with increased distance from the outcrop (Fig. 4). However, as block size reduces, a condition
417 is approached whereby the population of blocks are increasingly those which resist fracturing (see
418 section 'Block size controls) which should allow edge rounding to become more persistent and thus
419 more pronounced with distance. This condition may be approached in the case of the examples from
420 Teesdale (Fig. 4A) where it is evident that short chords become fewer with distance as larger values
421 of r_c begin to dominate the population. As blocks in transport can reorientate within the ice flow,
422 edge rounding has no effect on block shape, given the shape definition herein. However, if blocks are
423 not free to reorientate, a case not considered herein, the form of blocks can be significantly affected
424 by abrasion in place (Boulton 1974; Hallet, 1979).

425

426 Although a positive exponential function (Equation 2) describes the increase in the mean edge
427 rounding with distance from the source outcrop (Fig. 4A inset panel), the function must eventually
428 transition to a negative function as abraded smaller blocks inevitably are characterized by smaller radii
429 of curvature. This latter condition was not recorded within the current study and sampling at greater
430 distances from the source would be required to determine if this transition occurs. A block (*e.g.*, 1 m



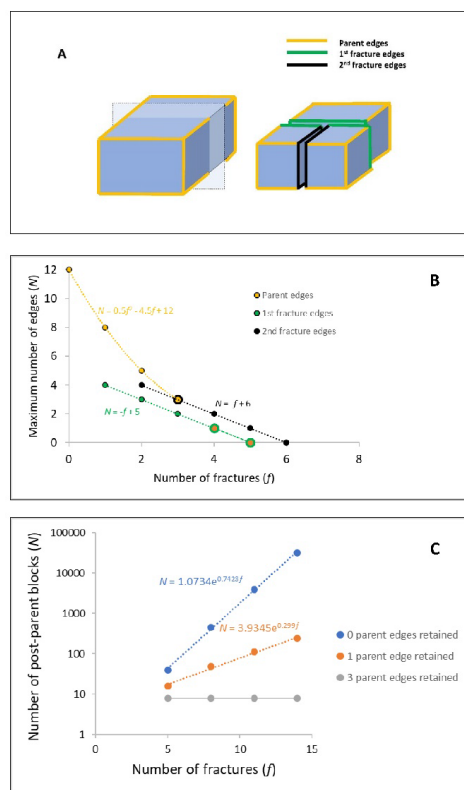
431 cube) subject to edge rounding equally on all 12 edges, as per Equation 2, would have lost about 4%
432 of its mass after 10 km and 9% after 40 km so, in contrast, fracture into two self-similar parts whereby
433 50% of mass is lost, is more significant than edge-rounding in terms of mass loss per block. The greater
434 significance of fracture is consistent with studies of ice erosion by quarrying versus abrasion of basal
435 bedrock surfaces (see references in Cohen *et al.*, 2006).

436

437 Rounding of individual blocks is not a steady process, as is evident from the data scatter in Fig. 4 and
438 is further illustrated in the following section. The process whereby the percentage of edges of
439 different generations are rounding with distance, or time, is shown schematically in Fig 8A, wherein
440 there are initially no more than 12 slightly rounded edges to a cube block newly released from outcrop
441 (see Supplementary Information for detail of the model). The model is simple but demonstrates the
442 complexity in edge rounding that must accompany successive fracturing of blocks. Fracturing the
443 block successively across the *L*-axis introduces new generations of fracture edges (sequent fractures
444 – Fig. 8B) at the same time as reducing the number of edges on each new block related to earlier
445 fracture events (see Supplementary Information for further detail). As the number of progeny blocks
446 increases exponentially for each fracture event (Fig. 8C), and each sibling can be further dissected
447 along one, two or three *M*-axes depending on block shape, a diagram including all fracture progeny
448 introduces unreasonable complexity, obscuring the key details. In Fig. 8A&B, for clarity, only one block
449 is followed through one to six sequent fractures, which reduces the number of data points for plotting
450 to a manageable number. The key point to illustrate is that the initial ‘parent’ block must be fractured
451 five times for one of the ensuing progenies to have lost all the initial 12 edges of the ‘parent’. The
452 total number of initial parent edges is relatively persistent because there are 12 edges to begin with
453 (Fig. 8). Contrarily, only four new edges (Fig. 8A) per block are produced on each fracture event. Thus,
454 in contrast to the curve for the initial parent edges, the 1st fracture edges can be lost in as little as four
455 fracture events depending on which sibling block is considered. The 2nd fracture edges are lost by a
456 total of five fracture events and so on, as more fractures occur adding new fracture edges. Relaxing



457 the model to allow fracture across either the M or S axis (see Supplementary Information) only adds
 458 one or two fracture events to the process of edge extinctions. Thus, by introducing new edges at each
 459 fracture event, rounding of the block with distance or time is not a steady progression, with well-
 460 rounded edges being lost as blocks are split at the same time as new immature edges are added to a
 461 population of sub-mature edges. The model may not apply beyond some undetermined number of
 462 fracture events if there is a critical minimum block size that is less susceptible to fracture (as was noted
 463 above) and rounding then can become pronounced. Nonetheless, this model explains the presence
 464 of a ‘continuum’ from well-rounded edges to less-well-rounded edges on many individual blocks. The
 465 issue as to whether there is a minimum block size is considered in the next section.



466

467 *Figure 8: A) A regular block released from outcrop has 12 initial edges (Parent edges) all equally*
 468 *rounded. Fracturing the block at right angles introduces four new edges (1st fracture edges) to each*
 469 *of two sibling blocks, which edges are younger than the initial edges. A further fracture across the L-*



470 *axis is indicated by 2nd fracture edges; B) The maximum number of edges of each generation on a*
471 *block as a function of the number of fracture events, with only the parent edges and those edges*
472 *related to the first two fracture events plotted; C) The total number of blocks created at each fracture*
473 *event which retain 0, 1 or 3 of the original parent edges.*

474

475 The significant mean edge rounding, with distance from outcrop (Fig. 4A inset panel), indicates that
476 the blocks were transported within a mobile concentration of basal debris, in frequent block-to-block
477 contact and in contact with the bedrock, leading to abrasion before being deposited within lodgement
478 till (Hallet, 1979). If the distance travelled towards the east and south is not the controlling factor,
479 then the high degree of edge-rounding may be due to prolonged temporal transport, with some
480 material moving east, south, and then north again, extending the transport distances. However,
481 compatible with studies showing block modification after distances of only 0.4 km (Humlum, 1985;
482 Lliboutry 1994; MacGregor *et al.* 2009), an alternative main explanation is preferred for the easterly
483 edge-rounding trend. Although Sg is mechanically strong in compression (Goudie, 2006) it is
484 susceptible to abrasion and tensile fracture for the following reason. The blocks contain large pink
485 phenocrysts set within a matrix of smaller mineral crystals. The large pink crystals are orthoclase
486 feldspar (Moh hardness 6 – 6.5). The other common minerals are glassy quartz (Moh hardness 7),
487 white plagioclase feldspar (Moh hardness 6) and black biotite mica (Moh hardness 2.5 – 3) (Caunt,
488 1986). Weathered examples of blocks often exhibit phenocrysts standing proud (3-5mm) of the matrix,
489 as the mica is readily subject to weathering (Wager, 1944). Thus, the granular composition of the
490 granite with harder crystals adjacent to a soft mineral may aid rapid rounding by abrasion and facilitate
491 tensile fracture during glacial transport.

492 **4.2 Block shape controls**

493

494 Block shape is dependent on the initial controls exhibited at: 1) the outcrop of origin; and 2) the
495 subsequent transport history.

496



497 1) The primary control is the intersection of sub-vertical joints (Firman, 1953) in the granite with
498 horizontal expansion joint planes caused by unloading (Jahnes, 1943). Horizontal joints largely are
499 due to glacio-isostatic rebound and surface erosion (Westaway, 2009), leading to the release of the
500 residual stresses accumulated at depth (Berger & Pitcher, 1970). The resultant blocks initially tend to
501 be cubic. Where blocks lie within a few metres from the parent outcrop, the block faces tend to be
502 planar, although curved fractured surfaces occur occasionally, as do conchoidal fracture hollows on
503 otherwise planar surfaces. Curved fracture surfaces tend to occur in homogeneous granite due to
504 pressure unloading (Wang *et al.*, 2022), which will have occurred as ice erosion reduced the
505 overburden. Such joint-defined blocks within an outcrop are readily entrained by moving ice (Matthes,
506 1930; Morland & Boulton, 1975).

507

508 2) Although inhomogeneous blocks in traction may be envisaged as breaking down into multiple
509 fragments at each compressive event (Boulton, 1978), the largely homogeneous nature of the Sg
510 lithology leads to simple tensile fracturing, at each breakage event, whereby subsequent generations
511 of blocks exhibit shapes largely similar to the parent forms. Thus, there is a tendency for equant blocks
512 to persist, through time and distance, due to the tensile stresses associated with flexure across the
513 stoss surfaces reducing block mass in accord with either the silver model or the stochastic model. This
514 trend is indicated by the fact that stronger plate-like blocks occur less frequently away from the pluton
515 in contrast to the general absence at distance of the weaker rod-like blocks. Thus, cuboids progress
516 to form both cubes and cuboids such that the initial hypothesis is rejected.

517

518 **4.3 Block size controls**

519

520 Block size is dependent on the initial controls exhibited at: 1) the outcrop of origin; and 2) the
521 subsequent transport history.

522



523 1) The primary control is the presence of the frequent, well-developed joint planes within the pluton
524 (Firman, 1953; Caunt, 1986) which tend to define and delimit the range of the initial block sizes from
525 c., 0.5 m to 4 m. Fault planes are of sufficient rarity to be ignored. Joints are largely orthogonal: *i.e.*,
526 sub-vertical and near horizontal but oblique joints also occur.

527

528 2) Once in ice-transport, other controls on block disintegration may pertain. In the present case,
529 larger blocks close to the outcrop (< 0.8 km) often exhibit one (or more) intact or partially opened
530 failure plane(s) inherited from the outcrop structure. More commonly, with distance from the outcrop
531 (> 0.8 km), the planes of failure within individual blocks represent the directions of tensile and
532 compressive forces exerted by the ice on the blocks (and thus bear no relationship to structure or
533 composition), as appears to be the case where failure planes are aligned with the *L* or *M* axes. Fracture
534 occurred when the effective tensile stress exceeded the yield strength of the blocks. Glacial unloading,
535 and subsequent stress release, also may introduce planes of weakness within transported blocks.
536 Adopting the stochastic fracture mode or the silver ratio model for block shape changes indicates that
537 block volume effectively halves at each fracture event with consequent reduction in block size. This
538 conclusion has implications for the fractal evolution of erratic size distributions which, for brevity,
539 cannot be addressed within this paper.

540

541 Other small-scale planes of weakness can be attributed to spatial variations in the primary mineral
542 composition (Grantham, 1928; Parsons & Lee, 2005) leading to textural and grain-size variations which
543 can be visible rarely as parallel lineaments, and later hydrothermal alteration also induced
544 compositional and hence structural variations (Caunt, 1986). These weaknesses lead to loss of small
545 blocks and flakes from the larger parent blocks (see Supplementary Information) through spallation
546 rather than fracture. Spallation may be related to the state of stress within a deforming till layer
547 (LeBone Hooke & Iverson, 1995) rather than the tensile stress on the stoss side of a block which
548 accounts for block fracture.



549

550 **4.4 General considerations**

551

552 A significant question is whether flowing ice can generate significant stress to fracture the granite
553 blocks. In a consideration of similar situations, emphasis was placed on the compressive strengths of
554 blocks (Boulton, 1978) relative to the normal stresses due to a static ice load above a block. In the
555 present examples, the tensile strength of the stoss side of a block resisting flexure is more relevant for
556 brittle fracture and for granite can be as low as 8 MPa, which is a tensile stress readily applied by a
557 modest yet dynamic ice cover (Hallet, 1996). The distribution of compressive and tensile forces over
558 the stoss side of a block adjacent to the bedrock at the base of an ice mass will be complex and variable
559 through space and time (Hallet, 1979; Morland & Boulton, 1975; Ficker *et al.*, 1980; Cohen *et al.*, 2005).
560 Yet, a simple example below outlines the principles within the context of Shap granite erratics.

561

562 Setting the tensile stress at failure to 8 MPa and treating the rectangular block as subject to a critical
563 average driving force (τ_c) (Benn & Evans, 2011, p.114) due to ice flow, transverse and longitudinal
564 shear stresses arise of equal magnitude. Setting the fracture focus at half the block width in the
565 direction of loading, neglecting any water pressure variations (Cohen *et al.*, 2006) and deformation
566 within a basal till (LeBone Hooke & Iverson, 1995), and imposing the driving stress transverse to the
567 fracture plane, as little as 180 m thickness (H) of flowing glacial ice with an ice surface slope (α) of 1.5°
568 would be sufficient to induce fracture in the block:

569

$$570 \quad \tau_c = \rho_i g H \tan \alpha, \quad (3)$$

571

572 where ρ_i is the density of glacial ice and g is the acceleration due to gravity. The value of $H = 180$ m
573 pertains for a rectangular block with a surface area (A) defined by $L = 2$ m and $M = 2$ m (see
574 Supplementary Information for details). The effective instantaneous stress might be greater than as



575 given by Equation 3 (LeBone Hooke & Iverson, 1995) but for a block with $L = 3$ m, $M = 1$ m with the
576 long axis transverse to the ice flow the shear force maximum might be achieved with only 130 m of
577 ice cover (see Supplementary Information). To the east of the pluton the Last British Ice Sheet was
578 several hundred metres thick *c.*, 25-22 ka BP (Evans *et al.*, 2009), such that blocks would readily
579 fracture during full-glacial conditions, as well as after the Late Glacial Maximum when ice was thinning.
580

581 The smallest block sizes ($L < c.$, 1.0 m) present in the field were not considered, which means that the
582 sampled population was truncated at the finer end. Nevertheless, although in some rock-types, a
583 lower limit to block strength may be related to a minimum structural block size (Dreimanis & Vagners,
584 1971; Lim *et al.*, 2004; Domokos *et al.*, 2015) this is unlikely to pertain to granite which breaks-down
585 to grus at the scale of the phenocrysts. None-the-less, fracture and surface wear, to an initial block
586 population, tend to result in the observed block population consisting of those blocks which are
587 strongly resistant to further comminution (Moss, 1972; Tavares and King, 1998; Larson & Mooers,
588 2004; Pfeiffer *et al.*, 2022) which, in principle, enables some blocks to survive transport adjacent to
589 the sole of the ice for great distances before being deposited during the waning phase of the easterly
590 directed ice stream (Hallet, 1979). Thus, although there may be no lower effective block size, a
591 statistical increase in resistance to fracture of the block population with distance is likely evident as
592 witnessed by the increased rounding seen in the Teesdale population. The occasional far-travelled
593 large block, as noted in the Introduction, might be explained as being a statistically stronger example,
594 in contrast to the remainder of the population. Alternatively, large blocks can be cushioned within
595 the till body by smaller particles (Einav, 2007) thus avoiding fracture, or they can be transported
596 englacially, rather than basally, and consequently not subject to protracted abrasion and significant
597 compression whilst in traction. However, englacial blocks are more likely to be angular (Shilts, 1976;
598 Boulton, 1978) and might retain rugose faces.

599



600 Thus, although the reduction in plume parameters values, such as block size and concentration, are
601 commonly viewed as exponential functions of distance from the source (Shilts, 1976), such models
602 (*e.g.*, Fig. 4A inset panel) consider the sampled population as a whole and the inferences derived may
603 not apply to the transport history of individual blocks. Certainly, the reduction in edge rounding for
604 individual blocks is irregular with distance.

605

606 **5 Conclusions**

607

608 The hypothesis that granite blocks would display an increase in edge rounding with distance from the
609 source outcrop is confirmed, whilst the hypothesis that shape would evolve with distance is refuted.
610 Although the mean value for edge rounding for the whole block population increases exponentially
611 with distance, edge rounding on individual blocks is an irregular function mediated by block fracture
612 mechanics, as block size reduces (with shapes fluctuating between cuboids, slabs and rods) with
613 distance and new sharp edges are provided to partially edge-rounded blocks. Thus, edge rounding,
614 and shape coevolve as block size is reduced. Fracture transverse to block orientation is in accord with
615 the application of tensile stress which controls the process by which block form is conserved as block
616 size is reduced. Consideration of the orientation of the tensile fractures on blocks in the field might
617 be used to approximate the direction of ice flow at the time of fracture.

618

619 Overall, the results indicate that edge rounding is unlikely to be advanced if blocks continue to fracture.
620 Well-rounded blocks must represent blocks that have resisted splitting. In the case of exceptionally
621 large, rounded blocks, the rock mass likely is unusually homogeneous, lacking potential fracture lines.
622 However, smaller blocks are less likely to contain potential fracture lines and so fracture should
623 become less prevalent as blocks reduce in size, which then promotes edge rounding.

624



625 Future work should consider developing mathematical models that represent the function of edge
626 rounding as predicated by a model (e.g., silver ratio) describing block size reduction. Similar studies
627 considering other lithologies (e.g., stratified sedimentary rocks) likely would find different shape
628 evolution patterns in contrast to the cuboid central tendency displayed by the homogeneous granite,
629 with concomitant implications for edge rounding trends with time and distance.

630

631 **Author contribution**

632

633 PAC designed the study and conducted the field work, analysis, interpretation and drafting.

634

635 **Competing interests**

636

637 The author declares that he has no conflict of interest.

638

639 **Acknowledgements**

640

641 Emma Armstrong (Armstrongs Group) for access to the Shap (Pink) Quarry. Leslie Knight and David

642 Evans (Durham University) provided information on the location of Shap granite erratics in Teesdale

643 and near Levy Pool. Leslie Knight provided the base image for Fig. 3A.

644 **Data Availability**

645 Basic data are available upon reasonable request from the author.

646

647 **References**

648

649 Anikoh, G.A., Adesida, P.A., Afolabi, O.C.: Investigation of physical and mechanical properties of
650 selected rock types in Kogi State using hardness tests. *Journal of Mining World Express*, 4, 37-51.

651 DOI:10.14355/mwe.2015.04.004, 2015.

652



- 653 Benn, D.I.: The genesis and significance of 'Hummocky Moraine': Evidence from the Isle of Skye,
654 Scotland. *Quaternary Science Reviews*, 11, 781-799. [https://doi.org/10.1016/0277-3791\(92\)90083-K](https://doi.org/10.1016/0277-3791(92)90083-K),
655 1992.
- 656
- 657 Benn, D.I., Evans, D.J.A.: *Glaciers and Glaciation*, Hodder, London. 802pp,
658 <https://doi.org/10.1111/j.1502-3885.2011.00212.x>, 2011.
- 659
- 660 Berger, A.R., Pitcher, W.S.: Structures in granitic rocks: A commentary and a critique on granite
661 tectonics. *Proceedings of the Geological Association of London*, 81, 441-461.
662 [https://doi.org/10.1016/S0016-7878\(70\)80006-2](https://doi.org/10.1016/S0016-7878(70)80006-2), 1970.
- 663
- 664 Bouchard, M.A., Salonen, V.-P.: Block transport in shield areas, *Glacial Indicator Trains*, Kujansuu, R.,
665 Saarnisto, M., (editors), Balkema, Rotterdam, 87-107, ISBN 9781003079415, 1990.
- 666
- 667 Boulton, G.S.: Processes and patterns of glacial erosion. *Glacial Geomorphology*, Coates, D. R.,
668 editor), Binghamton, N.Y., State University of New York, 41-87, Publications in Geomorphology,
669 ISBN: 9789401164931, 1974.
- 670
- 671 Boulton, G.S.: Boulder shapes and grain-size distributions of debris as indicators of transport paths
672 through a glacier and till genesis. *Sedimentology*, 25, 773-799. [https://doi.org/10.1111/J.1365-](https://doi.org/10.1111/J.1365-3091.1978.TB00329.X)
673 [3091.1978.TB00329.X](https://doi.org/10.1111/J.1365-3091.1978.TB00329.X), 1978.
- 674
- 675 British Standard Institution: Code of Practice for Site Investigations, BS 5930
676 HMSO, London, 1981.
- 677
- 678 Buscarnera, G., Einav, I.: The mechanics of brittle granular materials with coevolving grain size and
679 shape. *Proceedings of the Royal Society, A*, 477: 20201005. <https://doi.org/10.1098/rspa.2020.1005>,
680 2021.
- 681
- 682 Carling, P.A., Su, T., Meshkova, L.: Distribution of Devensian glacial erratics and related evidence
683 elucidate complex ice flow changes across a former ice divide: Northern England. *Proceedings of the*
684 *Geologists' Association*, 134, 139-165. <https://doi.org/10.1016/j.pgeola.2023.01.002>, 2013.
- 685
- 686 Caunt, S.L.: *Igneous and Metamorphic Processes in the Shap Granite and its Aureole*. Unpubl. PhD
687 thesis, University of Leeds, 337pp, <https://etheses.whiterose.ac.uk/522/>, 1986.
- 688
- 688 Clark, P.U., Dyke, A.S., Shakun, J.D., Carlson, A.E., Clark, J., Wohlfarth, B., Mitrovica, J.X., Hostetler,
689 S.W., McCabe, M.: The Last Glacial Maximum. *Science*, 325, 710-714.
690 <https://doi.org/10.1126/science.1172873>, 2009.
- 691
- 692 Cohen, D., Iverson, N.R., Hooyer, T.S., Fischer, U.H., Jackson, M., Moore, P.L.: Debris-bed friction of
693 hard-bedded glaciers. *Journal of Geophysical Research*, 110, doi:10.1029/2004JF000228, 2005.
- 694
- 695 Cohen, D., Hooyer, T.S., Iverson, N.R., Thomason, J.F., Jackson, M.: Role of transient water pressure
696 in quarrying: A subglacial experiment using acoustic emissions. *Journal of Geophysical Research*, 111,
697 F03006, doi:10.1029/2005JF000439, 2006.
- 698
- 699 Demirdag, S., Sengun, N., Ugur, I., Altindag, R.: Estimating the uniaxial compressive strength of rocks
700 with Schmidt rebound hardness by considering the sample size. *Arabian Journal of Geosciences*, 11,
701 502, <https://doi.org/10.1007/s12517-018-3847-1>, 2018.
- 702



- 703 Domokos, G, Kun, F, Sipos, A.A., Szabó, T.: Universality of fragment shapes. *Scientific Reports*, 5,
704 9147. doi:10.1038/srep09147, 2015.
- 705 David J.A. Evans, D.J.A., Livingstone, S.J., Vieli, A., O' Cofaigh, C.: The palaeoglaciology of the central
706 sector of the British and Irish Ice Sheet: reconciling glacial geomorphology and preliminary ice sheet
707 modelling. *Quaternary Science Reviews*, 28, 739-757. doi:10.1016/j.quascirev.2008.05.011, 2009.
- 708 Dreimanis, A., Vagners, U.J.: Bimodal distributions of rock and mineral fragments in basal tills. Till: A
709 Symposium, Goldthwait, R.P. (Editor), Ohio State University Press, Columbus, 237-250, ISBN
710 9780814201480 1971.
- 711 Einav, I.: Breakage mechanics -Part 1: Theory. *Journal of Mechanics and Physics of Solids*, 55, 1274-
712 1297. <https://doi.org/10.1016/j.jmps.2006.11.003>, 2007.
- 713 Engineering ToolBox: *Compression and Tension Strength of some Common Materials*. [online]
714 Available at: https://www.engineeringtoolbox.com/compression-tension-strength-d_1352.html,
715 2008 [Accessed 02 01 2023].
- 716 Evans, D.J.A.: Glacial erratics and till dispersal indicators. *Encyclopaedia of Quaternary Science*, S.A.
717 Elias (Editor), Elsevier, Oxford, 975-978, ISBN 978-0-444-52747-9, 2007.
- 718 Firman, R. J.: *Metamorphism and Metasomatism around the Shap and Eskdale granites*, Durham
719 theses, Durham University. <http://etheses.dur.ac.uk/9565/>, 1953.
- 720 Ficker, F., Sonntag, G., Weber, E.: Asätze zur mechanischen deuring der rissentstehung bei
721 parablrisen und sichelbrüchen auf glaziageformten felsoberflächen. *Zeitschrift für Gletscherkunde
722 und Glazialgeologie*, 16, 25-43, 1980.
- 723
724 Glasser, N.F.; Roman, M.; Holt, T.O.; Žebre, M.; Patton, H.; Hubbard, A.L.: Modification of bedrock
725 surfaces by glacial abrasion and quarrying: Evidence from North Wales. *Geomorphology*, 365,
726 107283. <https://doi.org/10.1016/j.geomorph.2020.107283>, 2020.
- 727
728 Goudie, A.S.: The Schmidt Hammer in geomorphological research. *Progress in Physical Geography*,
729 30, 703-718. <https://doi.org/10.1177/0309133306071954>, 2006.
- 730
731 Grantham, D.R.: The petrology of the Shap Granite. *Proceedings of the Geological Association*, 39,
732 299-331. [https://doi.org/10.1016/S0016-7878\(28\)80015-0](https://doi.org/10.1016/S0016-7878(28)80015-0), 1928.
- 733
734 Haldorsen, S.: Grain-size distribution of subglacial till and its relation to glacial crushing and abrasion.
735 *Boreas*, 10, 91-105. <https://doi.org/10.1111/j.1502-3885.1981.tb00472.x>, 1981.
- 736
737 Hall, A.M., Mathers, H., Krabbendam, M.: Glacial ripping in sedimentary rocks: Loch Eriboll, NW
738 Scotland. *Geosciences*, 11, 232. <https://doi.org/10.3390/geosciences11060232>, 2021.
- 739
740 Hallet, B.: A theoretical model of glacial abrasion. *Journal of Glaciology*, 23, 39-50.
741 <https://doi.org/10.3189/S0022143000029725>, 1979.
- 742
743 Hallet, B.: Glacial abrasion and sliding: Their dependence on the debris concentration in basal ice.
744 *Annals of Glaciology*, 2, 23-28. <https://doi.org/10.3189/172756481794352487>, 1981.
- 745



- 746 Hallet, B.: Glacial quarrying: a simple theoretical model. *Annals of Glaciology*, 22, 1-8.
747 <https://doi.org/10.3189/1996AoG22-1-1-8>, 1996.
748
- 749 Hiramatsu Y, Oka Y.: Determination of the tensile strength of rock by a compression test
750 of an irregular test piece. *International Journal of Rock Mechanics and Mining Sciences &*
751 *Geomechanic Abstracts*, 3, 89–90. doi:10.1016/0148-9062(66)90002-7, 1966.
752
- 753 Hodgson, E.: The granite drift of Furness. *Geological Magazine*, 7, 328-339.
754 <https://doi.org/10.1017/S0016756800209801>, 1870.
755
- 756 Holland, E.G.: Shap Granite. *Mine & Quarry Engineering*, 25, 2-15, 1959.
757
- 758 Hopkins, W.: On the transport of erratic blocks. *Transactions of the Cambridge Philosophical Society*,
759 8, 220-240, 1849.
760
- 761 Humlum, O.: Changes in texture and fabric of particles in glacial traction with distance from source,
762 Myrdalsjokull, Iceland. *Journal of Glaciology*, 31 (108), 150-156.
763 <https://doi.org/10.3189/S0022143000006390>, 1985.
764
- 765 Jahns, R. H.: Sheet structure in granites, its origin and use as a measure of glacial erosion in New
766 England. *Journal of Geology*, 51, 71– 98, 1943.
767
- 768 Kujansuu, R., Saarnisto, M.: Glacial Indicator Tracing, Balkema, Rotterdam, 252pp, ISBN
769 9781003079415, 1990.
770
- 771 Larson, P. C. & Mooers, H. D.: Glacial indicator dispersal processes: a conceptual model.
772 *Boreas*, 33, 238–249. DOI 10.1080/03009480410001262, 2004.
773
- 774 Le Bone Hooke, R., Iverson, N.R.: Grain-size distribution in deforming subglacial tills: Role of grain
775 fracture. *Geology*, 23, 57-60. [https://doi.org/10.1130/0091-](https://doi.org/10.1130/0091-7613(1995)023%3C0057:GSDIDS%3E2.3.CO;2)
776 [7613\(1995\)023%3C0057:GSDIDS%3E2.3.CO;2](https://doi.org/10.1130/0091-7613(1995)023%3C0057:GSDIDS%3E2.3.CO;2), 1995.
777
- 778 Li, X.F., Li, H.B., Zhang, Q.B., Jiang, J.L., Zhao, J.: Dynamic fragmentation of rock material:
779 Characteristic size, fragment distribution and pulverization law. *Engineering Fracture Mechanics*,
780 199, 739-759. <https://doi.org/10.1016/j.engfracmech.2018.06.024>, 2018.
781
- 782 Lim, W.L., McDowell, G.R., Collop, A.C.: The application of Weibull statistics to the
783 strength of railway ballast. *Granular Matter*, 6, 229–237. [http://dx.doi.org/10.1007/s10035-004-](http://dx.doi.org/10.1007/s10035-004-0180-z)
784 [0180-z](http://dx.doi.org/10.1007/s10035-004-0180-z), 2004.
785
- 786 Lliboutry, L.L.: Monolithologic erosion of hard beds by temperate glaciers. *Journal of Glaciology*, 40,
787 433-450. <https://doi.org/10.3189/S0022143000012314>, 1994.
788
- 789 Livingstone, S.J., Evans, D.J.A., Ó Cofaigh, C., Davies, B.J., Merritt, J.W., Huddart, D., Mitchell, W.A.,
790 Roberts, D.H., Yorke, L.: Glaciodynamics of the central sector of the last British-Irish Ice Sheet in
791 Northern England. *Earth-Science Reviews*, 111, 25-55.
792 <https://doi.org/10.1016/j.earscirev.2011.12.006>, 2012.
793
- 794 MacGregor, K., Anderson, R.S., Waddington, E.D.: Numerical modeling of glacial erosion and
795 headwall processes in alpine valleys. *Geomorphology*, 103, 189–204.
796 <https://doi.org/10.1016/j.geomorph.2008.04.022>, 2009.



- 797 Man, K., Wang, K., Liu, X.: Dynamic tensile properties of granite varied with depths under a similar
798 loading rate. *Advances in Civil Engineering*, Article ID 6048312,
799 <https://doi.org/10.1155/2018/6048312>, 2018.
- 800 Matthes, F. E.: Geological history of the Yosemite Valley. U.S. Geological Survey. Professional Paper
801 160, 160pp, 1930.
802
- 803 Merritt, J.W., Hall, A.M., Gordon, J.E., Connel, E.R.: Late Pleistocene sediments, landforms and events
804 in Scotland: a review of the terrestrial stratigraphic record. *Earth and Environmental Science*
805 *Transactions of the Royal Society of Edinburgh*, 110, 39-91.
806 <https://doi.org/10.1017/S1755691018000890>, 2019.
807
- 808 Morland, L.W., Boulton, G.S.: Stress in an elastic hump: the effects of glacier flow over elastic bedrock.
809 *Proceedings of the Royal Society, A*, 344, 157-173. <https://doi.org/10.1098/rspa.1975.0096>, 1975.
810
- 811 Moss, A.J.: Technique for assessment of blocks breakage in natural and artificial
812 environments. *Journal of Sedimentary Petrology*, 42, 725–728. [https://doi.org/10.1306/74D7261C-](https://doi.org/10.1306/74D7261C-2B21-11D7-8648000102C1865D)
813 [2B21-11D7-8648000102C1865D](https://doi.org/10.1306/74D7261C-2B21-11D7-8648000102C1865D), 1972.
814
- 815 Nicolson, H.A.: On the granite of Shap, in Westmoreland. *Transactions of the Edinburgh Geological*
816 *Society*, 1, 133-37, 1868, <https://doi.org/10.1144/transed.1.2.133>, 1868.
817
- 818 Oakey, R.J., Green, M., Carling, P.A., Lee, M.W.E., Sear, D.A., Warburton, J.: Grain-shape analysis– A
819 new method for determining representative blocks shapes for populations of natural grains. *Journal*
820 *of Sedimentary Research*, 75, 1065-1073. <https://doi.org/10.2110/jsr.2005.079>, 2005.
821
- 822 Olsen, L.: A method for determining total block roundness in sediments. *Boreas*, 12, 17-21.
823 <http://dx.doi.org/10.1111/j.1502-3885.1983.tb00355.x>, 1983.
824
- 825 Pfeiffer, A. M., Morey, S., Karlsson, H. M., Fordham, E. M., & Montgomery, D. R.: Survival of the
826 strong and dense: Field evidence for rapid, transport-dependent bed material abrasion of
827 heterogeneous source lithology. *Journal of Geophysical Research: Earth Surface*, 127,
828 e2021JF006455. <https://doi.org/10.1029/2021JF006455>, 2022.
829
- 830 Parsons I., Lee, M.R.: Minerals are not just chemical compounds. *The Canadian Mineralogist*, 43,
831 1959-1992. <https://doi.org/10.2113/gscanmin.43.6.1959>, 2005.
832
- 833 Riley, J.M.: Glaciation of the Upper Eden Valley: a tale of wandering ice sheds. *Proceedings of*
834 *Westmorland Geological Society*, 28, 40-45, 2000.
835
- 836 Seo, D., Sohn, C., Cil, M.B., Buscarnera, G.: Evolution of blocks morphology and mode of fracture
837 during the oedometric compression of sand. *Géotechnique*, 71, 853-865.
838 <https://doi.org/10.1680/jgeot.18.P.300>, 2021.
839



- 840 Shilts, W.W.: Glacial till and mineral exploration. *Glacial Till, An Interdisciplinary Study*, R.F. Legget
841 (editor), Royal Society of Canada, Special Publication, 12, 205-224,
842 <https://doi.org/10.2136/sssaj1977.03615995004100010004x>, 1976.
843
844 Shipway P, Hutchings I.: Fracture of brittle spheres under compression and impact
845 loading. I. Elastic stress distributions. *Philosophical Magazine, A* **67**, 1389–1404.
846 <https://doi.org/10.1080/01418619308225362>, 1993.
847
848 Tavares, L.M., King, R.P.: Single-blocks fracture under impact loading. *International Journal of*
849 *Mineral Processing*, 54, 1–28. [https://doi.org/10.1016/S0301-7516\(98\)00005-2](https://doi.org/10.1016/S0301-7516(98)00005-2), 1998.
850
851 Ugelvig, S. V., Egholm, D.L., Iverson, N.R.: Glacial landscape evolution by subglacial quarrying:
852 A multiscale computational approach. *Journal of Geophysical Research: Earth Surface*,
853 121, doi:10.1002/2016JF003960, 2016.
854
855 Wager, L.R.: A stage in the decomposition of biotite from the Shap Granite. *Proceedings of the*
856 *Yorkshire Geological Society*, 25, 366-342, 1944.
857
858 Wang, X.-Y., Yin, Y.-C., Xing, M.-L., Zhang, D.-D., Chen, Y., Wang, E.-C.: Microsimulation study on
859 energy release and rock block ejection force of granite under different unloading conditions.
860 *Frontiers in Earth Science*, 10:909371. doi: 10.3389/feart.2022.909371, 2022.
861
862 Wentworth, C.K.: A method of measuring and plotting the shapes of pebbles. *US Geological Society*
863 *Bulletin* 730-C, 91-102. doi: 10.3133/B730C, 1923.
864
865 Westaway, R.: Quaternary uplift of northern England. *Global and Planetary Change*, 68, 357-382.
866 <https://doi.org/10.1016/j.gloplacha.2009.03.005>, 2009.
867
868 Wilson, P., Lord, T., Rodés, Á.: Deglaciation of the eastern Cumbria glaciokarst, northwest England,
869 as determined by cosmogenic nuclide (^{10}Be) surface exposure dating, and the pattern and
870 significance of subsequent environmental changes. *Cave and Karst Science*, 40, 22-27, 2013.
871
872 Zingg, T.: Beitrag zur schotteranalyse. PhD thesis, ETH Zurich, 1935.
873
874
875
876
877
878
879
880
881